

---

# BENCHMARKING OF FLATNESS-BASED CONTROL OF THE HEAT EQUATION

---

A PREPRINT

• **Stephan Scholz, Lothar Berger**  
Control and Process Engineering\*,  
University of Applied Sciences Ravensburg-Weingarten,  
Weingarten, Germany  
Email to: [stephan.scholz@rwu.de](mailto:stephan.scholz@rwu.de)

**Dirk Lebedez,**  
Institute of Numerical Mathematics,  
Ulm University,  
Ulm, Germany

August 1, 2023

## Abstract

Flatness-based control design is a well established method to generate open-loop control signals. Several articles discuss the application of flatness-based control design of (reaction-) diffusion problems for various scenarios. Beside the pure analytical derivation also the numerical computation of the input signal is crucial to yield a reliable trajectory planning. Therefore, we derive the input signal step-by-step and describe the influence of system and controller parameters on the computation of the input signal. In particular, we benchmark the control design of the one-dimensional heat equation with Neumann-type boundary actuation for pure aluminum and steel 38Si7, and discuss the applicability of the found input signals for realistic scenarios.

**Keywords** Heat Conduction · Feed-forward Control · Boundary Actuation

## 1 Introduction

The flatness-based control method is an open-loop technique to steer the system output along a reference trajectory [1]. In case of finite-dimensional linear and nonlinear systems the input signal  $u(t)$  is found by a finite number of derivatives of a (flat) output which equals the reference signal. This approach is extended to infinite-dimensional and distributed parameter systems where theoretically an infinite number of derivatives of output signal  $y(t)$  is necessary to compute the input signal [2, 3, 4]. However, for practical reasons we can only consider a finite number of derivatives of the output signal. Thus, we need to show that the computation of input signal  $u(t)$  converges for a certain number of derivatives of  $y(t)$ . In general, this estimation of convergence is not trivial because the computation of  $u(t)$  depends on system and control parameters.

In this contribution, we assume a one-dimensional linear heat equation with Neumann boundary actuation as depicted in Figure 1 to discuss the impact of system and control parameters on the computation of input signal  $u(t)$ . In particular, we compare pure aluminum and steel 38Si7 for this purpose. They differ in their material properties: thermal conductivity  $\lambda$ , specific heat capacity  $c$  and density  $\rho$ . Regarding the control parameters, we design the reference trajectory as a smooth step which is configured by the transition time and the steepness [5].

In section 2 we introduce the flatness-based modeling for the one-dimensional heat equation and derive input signal  $u(t)$ . The influence of the system parameters are analyzed in section 3. The trajectory planning problem and the subsequent discussion of the control parameters are described in section 4 and 5, respectively. Finally, in section 6 we present the simulation results of the open-loop system and review the applicability for realistic scenarios.

---

\*Web: <https://forschung.rwu.de/forschungsgruppen/control-and-process-engineering>

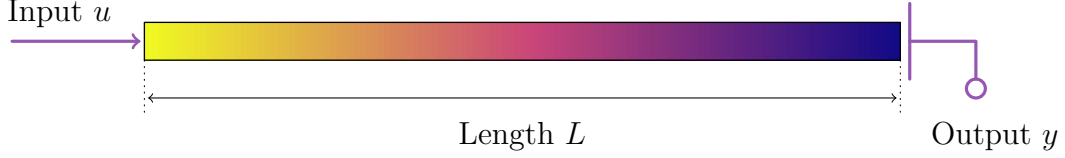


Figure 1: One-dimensional rod with heat input (left) and temperature measurement (right).

## 2 Flatness-based Control

We assume a one-dimensional heat conduction model as portrayed in Figure 1 with Neumann boundary actuation on the left side and a thermally insulated right side as

$$\dot{\vartheta}(t, x) = \alpha \frac{\partial^2}{\partial x^2} \vartheta(t, x) \quad , \quad (t, x) \in (0, T) \times (0, L), \quad (1)$$

$$u(t) = \lambda \left. \frac{\partial}{\partial x} \vartheta(t, x) \cdot \vec{n}_0 \right|_{x=0}, \quad (2)$$

$$0 = \lambda \left. \frac{\partial}{\partial x} \vartheta(t, x) \cdot \vec{n}_L \right|_{x=L} \quad (3)$$

where the outer normal vectors are known as  $\vec{n}_0 = -1$  and  $\vec{n}_L = 1$ . Here, we denote the temperature as  $\vartheta$ , the thermal conductivity as  $\lambda$  and the diffusivity as  $\alpha = \frac{\lambda}{c \rho}$  with specific heat capacity  $c$  and density  $\rho$ . The Neumann boundary conditions (2-3) are rough simplifications of rather realistic boundary conditions consisting of linear heat transfer and nonlinear heat radiation, e.g.

$$\lambda \left. \frac{\partial}{\partial x} \vartheta(t, x) \cdot \vec{n} \right|_{x \in \{0, L\}} = -h(\vartheta(t, x) - \vartheta_{amb}) - k(\vartheta(t, x)^4 - \vartheta_{amb}^4)$$

with constants  $h > 0$ ,  $k > 0$  and ambient temperature  $\vartheta_{amb}$ , see [6, 7]. However, such realistic boundary conditions lead to a much more complex mathematical discussion which is out of scope of this contribution. The initial temperature distribution is arbitrarily defined by

$$\vartheta(0, x) = \vartheta_0(x) \quad \text{for } x \in [0, L]$$

and the temperature is measured on the right boundary as

$$y(t) = \vartheta(t, L). \quad (4)$$

As known from the literature [2, 3, 4] the heat equation can be represented by a power series approach. So, we define power series

$$w(t, x) := \sum_{i=0}^{\infty} w_i(t) \frac{(L-x)^i}{i!}$$

and find its derivatives with respect to position  $x$  as

$$\begin{aligned} \frac{\partial}{\partial x} w(t, x) &= - \sum_{i=0}^{\infty} w_{i+1}(t) \frac{(L-x)^i}{i!} \quad \text{and} \\ \frac{\partial^2}{\partial x^2} w(t, x) &= \sum_{i=0}^{\infty} w_{i+2}(t) \frac{(L-x)^i}{i!}. \end{aligned} \quad (5)$$

We model heat equation (1) in terms of

$$\dot{w}(t, x) = \alpha \frac{\partial^2}{\partial x^2} w(t, x),$$

identify both sides by its power series expressions as

$$\sum_{i=0}^{\infty} \dot{w}_i(t) \frac{(L-x)^i}{i!} = \alpha \sum_{i=0}^{\infty} w_{i+2}(t) \frac{(L-x)^i}{i!}$$

and yield identity

$$\dot{w}_i(t) = \alpha w_{i+2}(t). \quad (6)$$

Next, we apply the information of both boundary sides on identity (6) to derive the input signal. Firstly, we consider the output signal (4) as

$$y(t) = w(t, L) = \sum_{i=0}^{\infty} w_i(t) \frac{0^i}{i!} = w_0(t)$$

which implies  $\frac{d^i}{dt^i} y(t) = \frac{d^i}{dt^i} w_0(t) = \alpha^i w_{2i}$  with identity (6). Secondly, the boundary condition on the right side (3) is formulated as

$$\lambda \frac{\partial}{\partial x} w(t, L) = -\lambda \sum_{i=0}^{\infty} w_{i+1}(t) \frac{0^i}{i!} = -\lambda w_1(t) = 0$$

and we find  $\frac{d^i}{dt^i} w_1(t) = \alpha^i w_{2i+1} \equiv 0$ . Thus, identity (6) is described by the sequences

$$w_{2i}(t) = \alpha^{-i} y^{(i)}(t) \quad \text{and} \quad w_{2i+1}(t) = 0 \quad (7)$$

for all  $n \in \{0, 1, \dots, \infty\}$ . In the definition of boundary actuation (2) we insert Equation (5) to derive the input signal  $u(t)$  as

$$u(t) = -\lambda \frac{\partial}{\partial x} w(t, 0) = \lambda \sum_{i=0}^{\infty} w_{i+1}(t) \frac{L^i}{i!}$$

and further with  $i \rightarrow 2i + 1$  and Equation (7) as

$$u(t) = \lambda \sum_{i=0}^{\infty} \frac{L^{2i+1}}{\alpha^{i+1}} \frac{1}{(2i+1)!} y^{(i+1)}(t). \quad (8)$$

### 3 Influence of System Parameters

We are interested in the sequence values of series (8) because for implementation reasons we need to know how much memory has to be reserved for the computation of  $u$  and at which iteration  $i$  the summation can be stopped. The power series to compute input signal  $u(t)$  can be separated in sequence

$$\eta_i = \frac{L^{2i+1}}{\alpha^{i+1}} \frac{1}{(2i+1)!}. \quad (9)$$

and the derivatives of the (desired) output signal  $y^{(i+1)}(t)$ . In this section we discuss the influence of the physical properties length  $L$  and diffusivity  $\alpha$  on sequence  $\eta_i$ , and in section 5 we analyze the parameters of (target) output  $y(t)$  and its derivatives.

Sequence  $\eta_i$  is positive for all  $i \in \{0, 1, \dots, \infty\}$  as we assume  $L > 0$ ,  $\alpha > 0$ , and has a crucial influence on the computation of the input function  $u$  because it scales the derivatives  $y^{(i+1)}$ . Thus, we need to know the approximate values of  $\eta_i$ . We use a rescaled version of sequence (9) as

$$\tilde{\eta}_i := \left( \frac{L^2}{\alpha} \right)^{i+1} \frac{1}{(2i+1)!} = \frac{\gamma^{i+1}}{(2i+1)!} = L \eta_i$$

where  $\gamma := \frac{L^2}{\alpha}$  to show that  $\eta_i$  and  $\tilde{\eta}_i$  increase up to some index  $i$  and decrease afterwards to zero. Increasing iterator  $i$  by one we yield

$$\tilde{\eta}_{i+1} = \frac{\gamma^{[i+1]+1}}{(2[i+1]+1)!} = \frac{\gamma^{i+1}}{(2i+1)!} \frac{\gamma}{(2i+2)(2i+3)} = \tilde{\eta}_i \beta_i$$

where  $\beta_i = \frac{\gamma}{(2i+2)(2i+3)}$  and we notice

$$\frac{\tilde{\eta}_{i+1}}{\tilde{\eta}_i} > 1 \quad \Leftrightarrow \quad \beta_i > 1 \quad \text{and} \quad \frac{\tilde{\eta}_{i+1}}{\tilde{\eta}_i} < 1 \quad \Leftrightarrow \quad \beta_i < 1.$$

Due to the definition of  $\tilde{\eta}$  this concept holds also for the original sequence (9) as  $\eta_{i+1} = \beta_i \eta_i$ . So, the maximum value of  $\tilde{\eta}_i$  and  $\eta_i$  and its corresponding iterations  $i_{max}$  depend only on  $\gamma$ . For example, if we assume  $\gamma = 100$  then  $\gamma < (2i+2)(2i+3)$  holds for  $i \in \{1, 2, 3\}$  and we find the maximum value  $\tilde{\eta}_4 = \frac{100^5}{9!} \approx 27557$ .

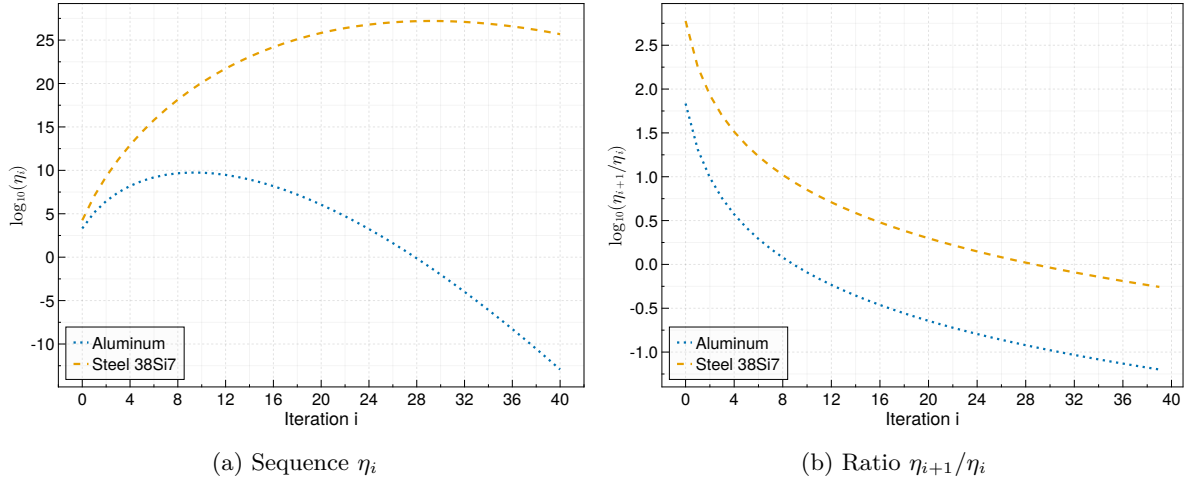


Figure 2: Sequence  $\eta_i$  (left) and ratio  $\frac{\eta_{i+1}}{\eta_i}$  (right) for aluminum and steel 38Si7.

### Example: Comparison Aluminum and Steel

For our numerical evaluations we consider a rod of length  $L = 0.2$  for two case scenarios: a rod made of pure aluminum [8] and a rod made of steel 38Si7 [9]. The physical properties of both materials are listed in Table 1. For aluminum we have  $\gamma_{al} \approx 410$  and for steel 38Si7 we have  $\gamma_{st} \approx 3588$ . The sequences  $\eta_{al,i}$  and  $\eta_{st,i}$  and their ratios  $\frac{\eta_{al,i+1}}{\eta_{al,i}}$  and  $\frac{\eta_{st,i+1}}{\eta_{st,i}}$  which describe evolution of the sequences by iteration are portrayed in Figure 2 in semi-logarithmic scaling. We find that inequality  $\frac{\eta_{i+1}}{\eta_i} > 1$  or equally  $\log_{10}\left(\frac{\eta_{i+1}}{\eta_i}\right) > 0$  holds in case of aluminum for  $i \in \{1, \dots, 8\}$  and in case of steel  $i \in \{1, \dots, 28\}$ . Thus the maximum values of  $\eta_i$  for aluminum and steel are calculated by

$$\eta_{al,9} = \frac{L^{19}}{\alpha_{al}^{10} 19!} \approx 5.53 \cdot 10^9 \quad \text{and} \quad \eta_{st,29} = \frac{L^{59}}{\alpha_{st}^{30} 59!} \approx 1.59 \cdot 10^{27}.$$

As both sequences  $\eta_{al,i}$  and  $\eta_{st,i}$  reach such enormous maximum values, computational issues related to big numbers and data types have to be considered in the implementation process.

Moreover, sequence  $\log_{10}(\eta_{al,i})$  drops below zero for  $i > 27$ :  $\eta_{al,28} \approx 0.73$ ,  $\log_{10}(\eta_{al,28}) \approx -0.13$ ; and  $\log_{10}(\eta_{st,i})$  drops below zero for  $i > 82$ :  $\eta_{st,83} \approx 0.13$ ,  $\log_{10}(\eta_{st,83}) \approx -0.87$  (not displayed in Figure 2).

## 4 Trajectory Planning

According to [4, 5] we consider a transition from one fixed operating point to the next one as

$$y(t) = y_0 + \Delta y \Phi_{\omega,T}(t) \tag{10}$$

where  $\Delta y = y_f - y_0$ , and with transition function

$$\Phi_{\omega,T}(t) = \begin{cases} 0 & t \leq 0, \\ 1 & t \geq T, \\ \frac{\int_0^t \Omega_{\omega,T}(\tau) d\tau}{\int_0^T \Omega_{\omega,T}(\tau) d\tau} & t \in (0, T) \end{cases}$$

Table 1: PHYSICAL PROPERTIES

	$\lambda$	$\rho$	$c$	$\alpha = \frac{\lambda}{\rho c}$
Aluminum	237	2700	900	$9.75 \cdot 10^{-5}$
Steel 38Si7	40	7800	460	$1.11 \cdot 10^{-5}$

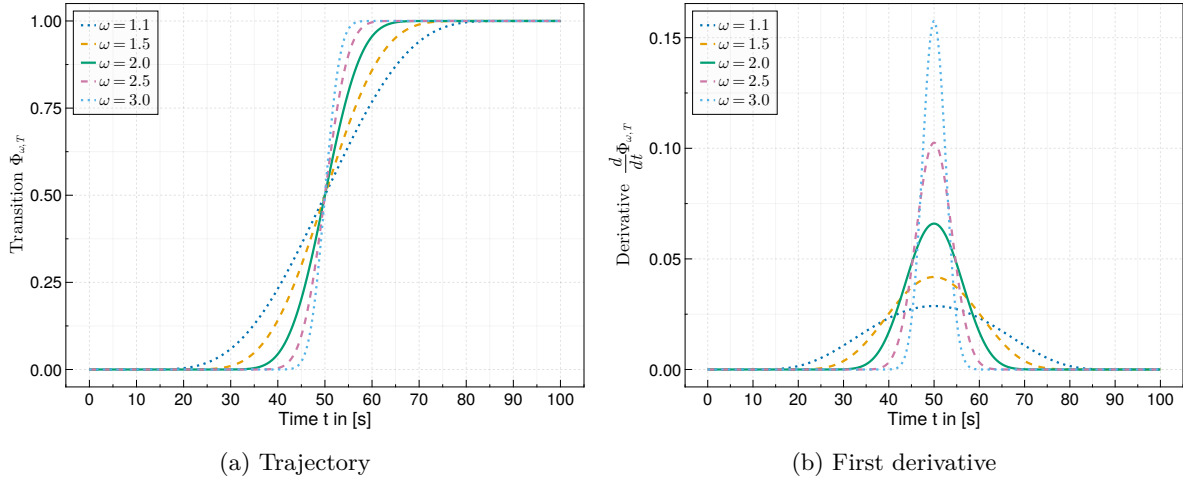


Figure 3: Trajectory  $\Phi_{\omega,T}$  (left) and its first derivative (right) with  $T = 100$  seconds and varying  $\omega \in \{1.1, 1.5, 2.0, 2.5, 3.0\}$ .

which uses the integral of the bump function

$$\Omega_{\omega,T}(t) = \begin{cases} 0 & t \notin [0, T], \\ \exp\left(-1/\left([1 - \frac{t}{T}]^{\frac{t}{T}}\right)^{\omega}\right) & t \in (0, T). \end{cases} \quad (11)$$

Parameter  $\omega$  steers the steepness of transition  $\Phi_{\omega,T}$  and is chosen such that the Gevrey order  $go = 1 + \frac{1}{\omega} < 2$  or equally  $\omega > 1$ . A small value of  $\omega$ , e.g.  $\omega = 1.1$  means a rather flat transition, whereas a large value, e.g.  $\omega = 3.0$  means a quite steep transition, as depicted in Figure 3. To compute the input signal  $u(t)$  in Equation (8) we only need to find the derivatives

$$\frac{d^i}{dt^i} y(t) = \Delta y \Phi_{\omega,T}^{(i)}(t) \quad (12)$$

where the derivatives of transition  $\Phi_{\omega,T}$  are calculated as

$$\Phi_{\omega,T}^{(i)}(t) = \frac{\Omega_{\omega,T}^{(i-1)}(t)}{\hat{\Omega}_{\omega,T}} \quad \text{for } t \in (0, T) \quad (13)$$

and  $\Phi_{\omega,T}^{(i)}(t) = 0$  for  $t \notin (0, T)$ , using integral

$$\hat{\Omega}_{\omega,T} := \int_0^T \Omega_{\omega,T}(\tau) d\tau. \quad (14)$$

In Figure 3 trajectory  $\Phi_{\omega,T}(t)$  and its first derivative are portrayed for varying  $\omega \in \{1.1, 1.5, 2.0, 2.5, 3.0\}$ . The derivatives  $\Phi_{\omega,T}^{(i)}(t)$  can be computed symbolically using for example computer-algebra systems (see for example the MATLAB implementation [10]), numerically (which we do not recommend here). In this contribution, we compute the derivatives  $\Omega_{\omega,T}^{(i)}$  with the JULIA library *BellBruno.jl* [11].

## 5 Influence of Control Parameters

The configuration of transition  $\Phi_{\omega,T}$  and its derivatives are mainly driven by two parameters: final time  $T$  and exponent  $\omega$ . In this section, we apply the  $L^2$  norm

$$\|f\|_{L^2} = \sqrt{\int_0^T |f(t)|^2 dt}$$

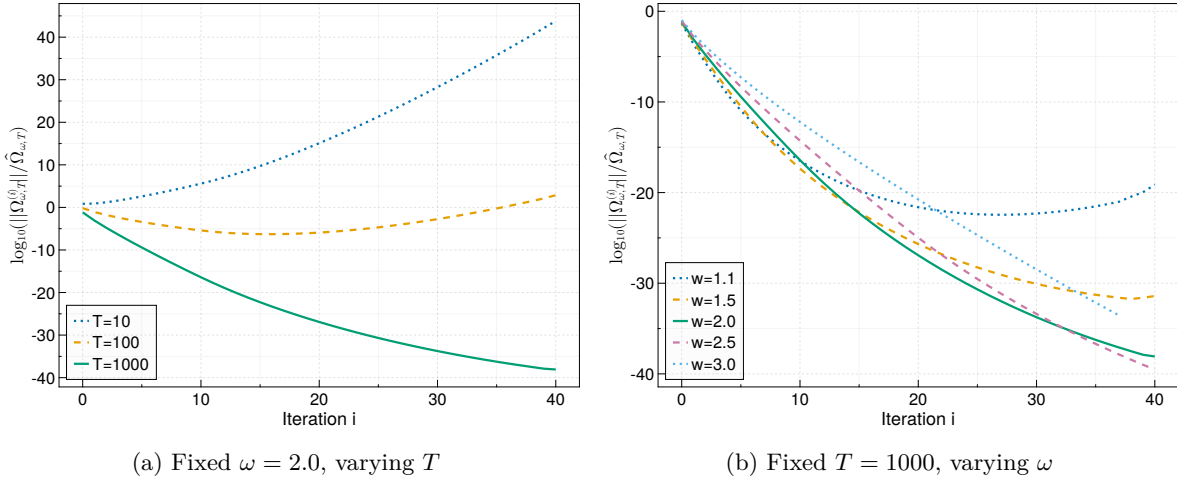


Figure 4: Norm of  $\Omega_{\omega,T}^{(i)}$  with fixed  $\omega = 2.0$  left, and fixed  $T = 1000$  right.

on  $\frac{d^i}{dt^i} \Omega_{\omega,T}(t)$  to unveil the influence of final time  $T$  and exponent  $\omega$  on the computation of input signal (8). Noting the input signal with sequence  $\eta_n$  as

$$u(t) = \lambda \sum_{i=0}^{\infty} \eta_i y^{(i+1)}(t) = \frac{\lambda \Delta y}{\hat{\Omega}_{\omega,T}} \sum_{i=0}^{\infty} \eta_i \Omega_{\omega,T}^{(i)}(t)$$

using identities (12,13,14), we find the  $L^2$  norm of  $u(t)$  as

$$\|u(t)\|_{L^2} = \left\| \frac{\lambda \Delta y}{\hat{\Omega}_{\omega,T}} \sum_{i=0}^{\infty} \eta_i \Omega_{\omega,T}^{(i)}(t) \right\| \leq |\Delta y| \frac{\lambda}{\hat{\Omega}_{\omega,T}} \sum_{i=0}^{\infty} \eta_i \|\Omega_{\omega,T}^{(i)}(t)\|$$

where we assume  $\lambda, \hat{\Omega}_{\omega,T}, \eta_i > 0$ . We see that the power series is mainly driven by  $\eta_i$  (as discussed before) and derivatives  $\Omega_{\omega,T}^{(i)}(t)$ . Therefore, we are able to describe the quantitative behavior of the input signal by evaluating sequence

$$\mu_i := \frac{\lambda |\Delta y|}{\hat{\Omega}_{\omega,T}} \eta_i \|\Omega_{\omega,T}^{(i)}(t)\|_{L^2}. \quad (15)$$

Scaled norm  $\|\frac{d^i}{dt^i} \Omega_{\omega,T}(t)\|_{L^2} / \hat{\Omega}_{\omega,T}$  is portrayed in Figure 4 in logarithmic scaling for two scenarios: fixed  $\omega = 2$  and varying  $T \in \{10, 100, 1000\}$ ; and fixed  $T = 1000$  and varying  $\omega \in \{1.1, 1.5, 2.0, 2.5, 3.0\}$ . One notes that an increasing value only of final time  $T$  leads to a reduction of  $\|\Omega_{\omega,T}^{(i)}(t)\| / \hat{\Omega}_{\omega,T}$ , the influence of steepness  $\omega$  may not be so clear here.

Furthermore, we take advantage of sequence  $\mu_i$  to find a suitable maximum iteration number  $i_{max}$  to terminate the power series of  $u(t)$  in Equation (8). Sequence  $\mu_i$  consists of  $\eta_i$  as defined in Equation (9) and so we distinguish aluminum and steel 38Si7 as noted in Table 1). The different values of  $\eta_i$  for aluminum and steel 38Si7 as in Figure 2 lead to different values of  $\mu_i$ : sequence  $\mu_i$  approaching zero *faster* in case of aluminum than steel 38Si7 as depicted in Figure 5 (a). Introducing the ratio  $\frac{\mu_i}{\max_{j \in \{1, \dots, i\}} \mu_j}$  we find that the sequence elements  $\mu_i$  vanish in case of aluminum for iterations approximately above  $i = 5$  whereas in case of steel 38Si7 it takes at least  $i = 12$  iterations - as portrayed in Figure 5 (b).

The evaluation of  $\mu_i$  and ratio  $\frac{\mu_i}{\max_{j \in \{1, \dots, i\}} \mu_j}$  unveils two facts about the generation of input signal  $u(t)$ . Comparing the results for aluminum and steel 38Si7, we find in case of aluminum that only the very first derivatives of  $\Phi_{\omega,T}$  are weighted by  $\eta_i$  and higher order derivatives have almost no influence on the computation of  $u(t)$ . Whereas in case of steel 38Si7 the weights of derivatives increase up to the fifth derivative so higher order derivatives (which tend to oscillatory behavior) influence the found input signal, too. We find an

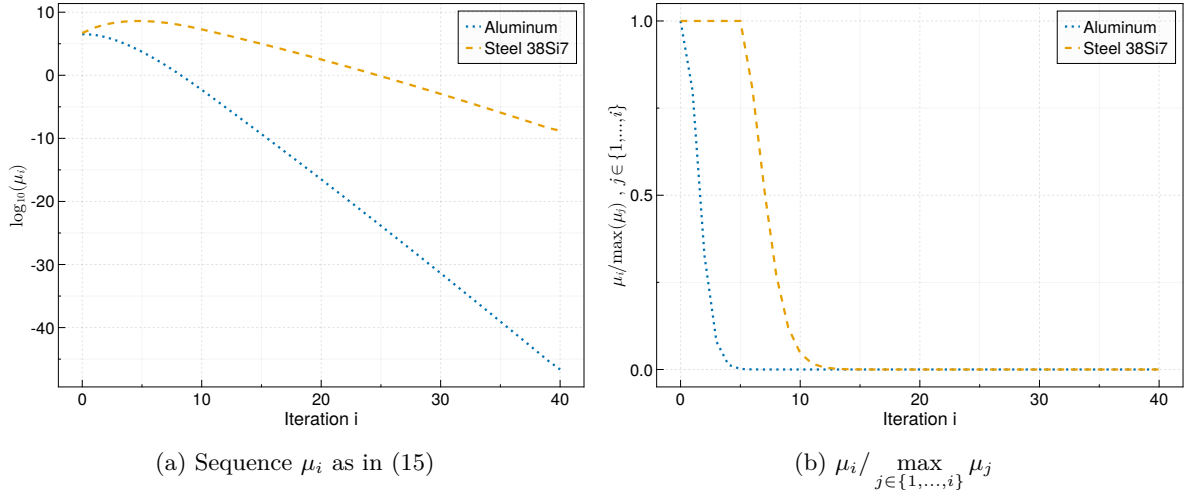


Figure 5: Sequence  $\mu_i$  and ratio  $\frac{\mu_i}{\max_{j \in \{1, \dots, i\}} \mu_j}$  for  $\omega = 2.0$  and  $T = 1000$ .

approximation of the signal input

$$u(t) \approx \frac{\lambda \Delta y}{\hat{\Omega}_{\omega, T}} \sum_{i=0}^N \eta_i \Omega_{\omega, T}^{(i)}(t) =: u_N(t) \quad (16)$$

where  $N \in \mathbb{N}_{\geq 0}$  denotes the upper limit of iterations. Following the previous ideas, in case of aluminum a small value of  $N$ , e.g.  $N = 7$ , suffices to generate a good approximation. However, for steel 38Si7 we need a higher number of iterations, e.g.  $N = 15$ . The progress of input signals for aluminum with  $N \in \{1, 3, 7\}$  and steel 38Si7 with  $N \in \{5, 10, 15\}$  are presented in Figure 6. These results confirm our previous analysis that the input signal needs fewer series elements for aluminum as for steel 38Si7.

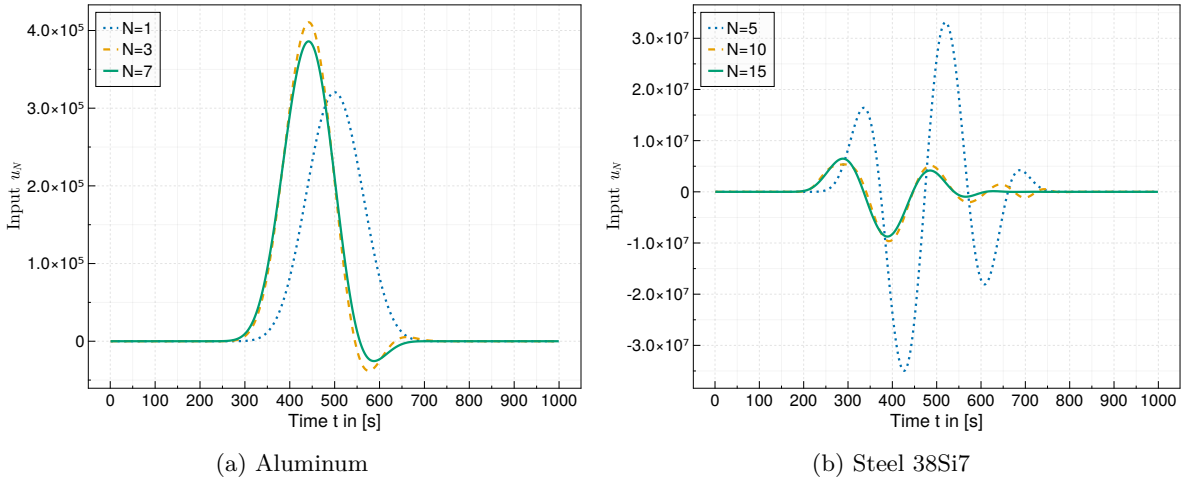


Figure 6: Progress of approximated input signals  $u_N$  for aluminum (left) and steel 38Si7 (right) with  $T = 1000$  and  $\omega = 2$ .

In a nutshell, we find four important parameters which influence the input signal: length of rod  $L$  and diffusivity  $\alpha$  which define sequence  $\eta_n$ , and final time  $T$  and steepness  $\omega$  which influences the derivatives of trajectory  $\Phi_{\omega, T}$  - and thus also the necessary number of summation iterations.

## 6 Simulation Results

In this section we compare the computed input signals and the resulting heat conduction simulation for aluminum and steel 38Si7. As above we assume the physical properties as listed in Table 1 and the trajectory parameters  $T = 1000$  seconds and  $\omega = 2.0$ . So, the integral of the bump function as in identity (14) is found as  $\hat{\Omega}_{\omega,T} \approx 17.06 \cdot 10^{-6}$ . Further, we assume an initial temperature  $\vartheta_0(x) = 300$  Kelvin which shall be increased by  $\Delta y = 100$  Kelvin. A maximum iteration number of  $N = 40$  is considered for approximation (16) in case of both scenarios. As explained in Section 5 lower values than  $N = 40$  are also sufficient but it may rather imitate a summation until  $N = \infty$ . Heat equation (1) is discretized in space using finite differences with 101 grid points and is simulated using the integration method *KenCarp4* (see [12]) from the JULIA library *OrdinaryDiffEq.jl* [13].

The input signals and the resulting temperatures are illustrated in Figure 7 for aluminum (a,c) and steel 38Si7 (b,d). In both cases the output, meaning the temperature at  $x = 0.2$  meter, follows the reference and reaches 400 Kelvin. So, from a pure *mathematical* point of view the input signals are computed correctly for both scenarios. However, from a *physical* or *technical* point of view we need to discuss the input signals and the resulting temperatures rather critically. Firstly, it may not be possible to apply negative input signals if the actuator offers only heating and not cooling. Secondly, it is physically not possible to reach temperatures below zero Kelvin as portrayed for steel reference in Figure 7 (d). Therefore, the control parameters final time  $T$  and steepness  $\omega$  have to be readjusted to yield physically sensible results.

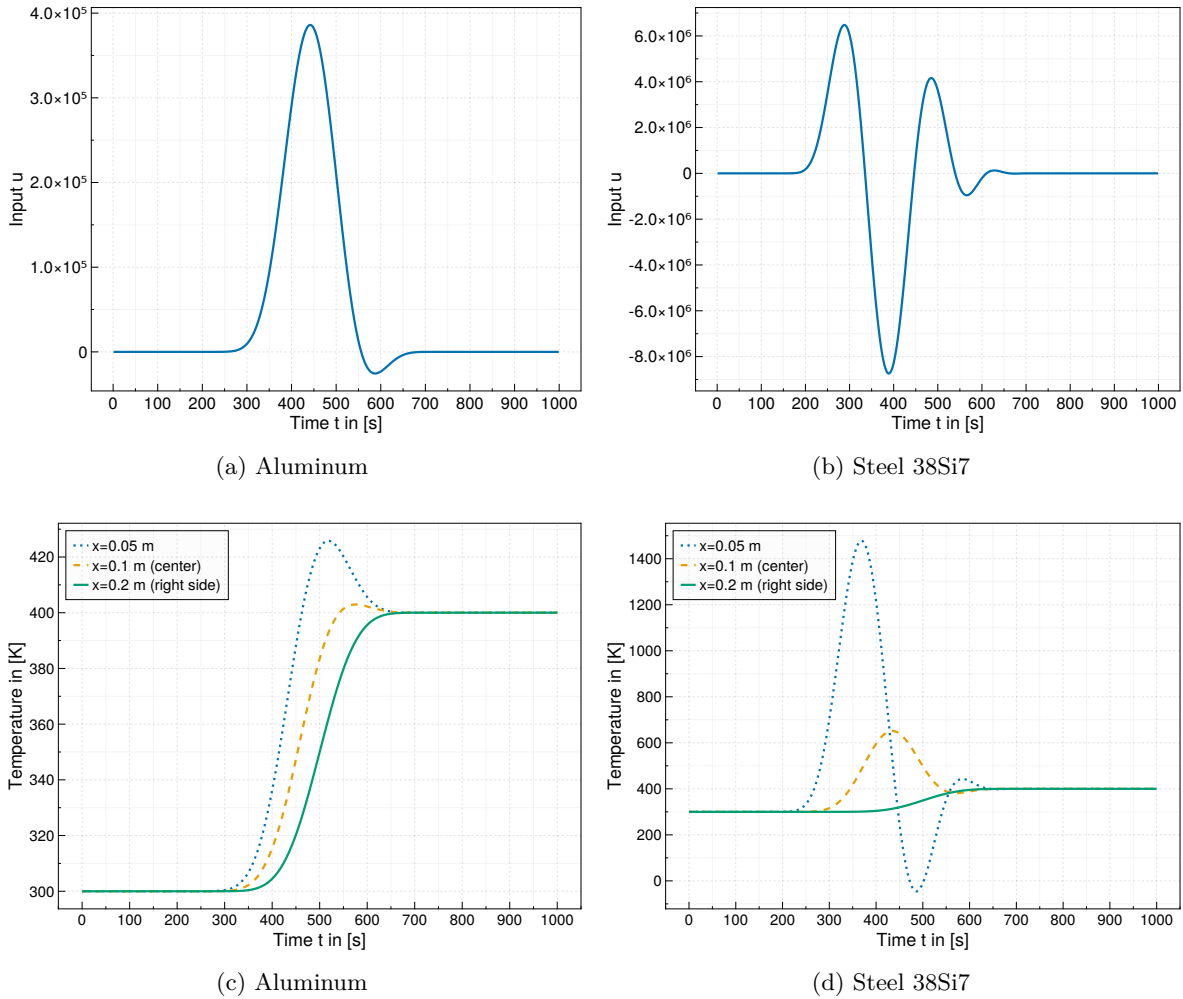


Figure 7: Input signals and the resulting temperatures at position  $x \in \{0.05, 0.1, 0.2\}$ .



## Source Code

The source code is developed in JULIA programming language and is available on *GitHub*:

<https://github.com/stephans3/BenchmarkFlatnessbasedControl.jl>

## Conclusion

In this article we presented the computation of input signals for trajectory planning of a one-dimensional heat equation using flatness-based control design. We analyzed the influence of system and control parameters on the computation of the input signal. So, we found that different material properties (aluminum, steel 38Si7) result in completely different input signals and open-loop dynamics even if all other parameters (length of rod, final time, steepness of transition) are the same. Moreover, our calculations and discussions demonstrate the complexity of flatness-based control of simplified realistic heat conduction problems. Further research on the evaluation of flatness-based control design with focus on rather realistic scenarios in two and three dimensions is necessary to gain a deeper insight of this complexity.

## References

- [1] Michel Fliess, Jean Lévine, Philippe Martin, Pierre Rouchon: *Flatness and defect of non-linear systems: introductory theory and examples*. International Journal of Control 61.6 (1995): 1327–1361.
- [2] Béatrice Laroche, Philippe Martin, Pierre Rouchon: *Motion planning for the heat equation*. International Journal of Robust and Nonlinear Control: IFAC-Affiliated Journal 10.8 (2000): 629–643.
- [3] François Ollivier, Alexandre Sedoglavic: *A generalization of flatness to nonlinear systems of partial differential equations. Application to the command of a flexible rod*. IFAC Proceedings Volumes 34.6 (2001): 219–223.
- [4] Joachim Rudolph, Jan Winkler, Frank Woittennek: *Flatness Based Control of Distributed Parameter Systems: Examples and Computer Exercises from Various Technological Domains*. Shaker, 2003.
- [5] Tilman Utz, Knut Graichen, Andreas Kugi: *Trajectory planning and receding horizon tracking control of a quasilinear diffusion-convection-reaction system*. IFAC Proceedings Volumes 43.14 (2010): 587–592.
- [6] Stephan Scholz, Lothar Berger: *Modeling of a multiple source heating plate*. arXiv preprint. arXiv:2011.14939 (2020).
- [7] Stephan Scholz, L. Berger: *Hestia.jl: A Julia library for heat conduction modeling with boundary actuation*. Simulation Notes Europe SNE 33.1 (2023): 27–30.
- [8] Periodic Table: *Aluminium – Periodic Table*. [Online]. Available: <https://www.periodic-table.org/Aluminium-periodic-table/>. [Accessed: Feb. 3, 2023].
- [9] Ovako: *38Si7*. [Online]. Available: <https://steelnavigator.ovako.com/steel-grades/38si7/>. [Accessed: Feb. 3, 2023].
- [10] Ferdinand Fischer, Jakob Gabriel, Simon Kerschbaum: *coni-a Matlab toolbox facilitating the solution of control problems*. Zenodo (2021). Available: <https://zenodo.org/record/6420876>.
- [11] Stephan Scholz: *BellBruno.jl*. Zenodo. 2023. Available: <https://doi.org/10.5281/zenodo.7685927>
- [12] Christopher A. Kennedy, Mark H. Carpenter: *Additive Runge-Kutta schemes for convection-diffusion-reaction equations*. Applied numerical mathematics 44.1-2 (2003): 139–181.
- [13] Rackauckas C, contributors. *SciML/DifferentialEquations.jl*. Zenodo. 2022. Available: <https://doi.org/10.5281/zenodo.7239171>